The Results of the Material Analysis of Artefacts Discovered at Zrínyi-Újvár and their Evaluation

Tibor Bartha

Introduction

As a result of investigations in the area of Zrínyi-Újvár, several artefacts of military significance have been discovered over the last decade, which, besides their historical significance, are also of archaeometallurgical interest. The vast majority of these finds were artillery and infantry projectiles and their shrapnel pieces, which can be connected to the 1664 Ottoman siege of Zrínyi-Újvár. The dating of the finds was greatly facilitated by the fact that there was only one siege in the area, namely the one in 1664. After the siege, the fortress (fortification)[1] was blown up by the Ottomans, and it was never rebuilt. Consequently, the mixing of finds connected to different sieges can be ruled out with absolute certainty.

Material analyses have already been carried out before 2018 on lead bullets,[2] cannonballs, mortar bombs, their shrapnel pieces, and the gunpowder filling of mortars discovered in the area of our research. The results of these investigations have already been published.[3]

During these earlier investigations, the primary objective was to gain an answer – occasionally only a confirmation – through the analysis of the chemical composition and macro- and microstructure of the samples about the materials and the technologies used for making the objects. We also investigated what specific characteristics of manufacturing can be identified or inferred in the case of each sample.

It opened a new phase in the investigations, when new finds connected to our subject were discovered in an octagonal, 15 m deep well, identified by drilling and ground penetrating radar surveying in 2016, which were excavated between 24 April and 26 May 2017. The well yielded not only the elements of the well house and well lining, planks, beams and other parts of the timber structure, but also a considerable amount of forged nails used for fitting the construction together. Many of the partially burnt, charred pieces of the timber well structure have remained in a very good condition and intact due to the preserving effect of the moist surroundings. There were also large numbers of musket balls of various diameters, sometimes concentrated.

---

1 Hereinafter: *fortress.*

2 Intact spherical and prism-shaped bullets, as well as bullets deformed as a result of impact.

3 *Bartha* 2013; *Bartha* 2017. It should be noted that although the latter study was already published in 2017, it predominantly presents the results gained by 2015.

https://doi.org/10.36250/00757_12

In 2018, the prime objective of our research was the archaeometric analysis of musket balls discovered during the excavation and the iron nails used for the construction of the well. Additionally, by studying the partially charred wooden remains, we came to the conclusion that the uncovered timber artefacts may also provide important information for the research. Therefore, we expanded the scope of our investigations to include the xylotomic analysis of the wooden material used for the well.

Archaeometric investigation of iron nails and lead musket balls from the archaeological excavation of Zrínyi-Újvár

Archaeometric analyses were carried out on three iron nails and three lead musket balls *(Figure 1).*[4]

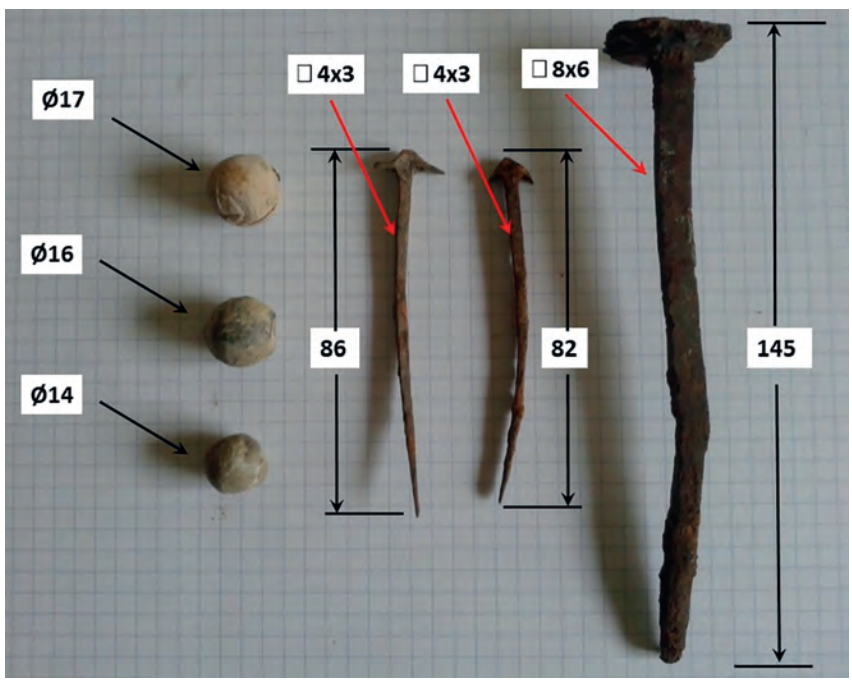

Figure 1.
The examined iron nails and lead musket balls in their original state
Source: Barkóczy–Török 2018.

[4] The examinations and the evaluation of the results were carried out by Dr. Péter Barkóczy and Dr. Béla Török, Archaeometallurgical Research Group of the University of Miskolc (ARGUM). *Barkóczi–Török* 2018.

Figure 2.
The examined iron nails after taking samples from them
Source: Barkóczy–Török 2018.

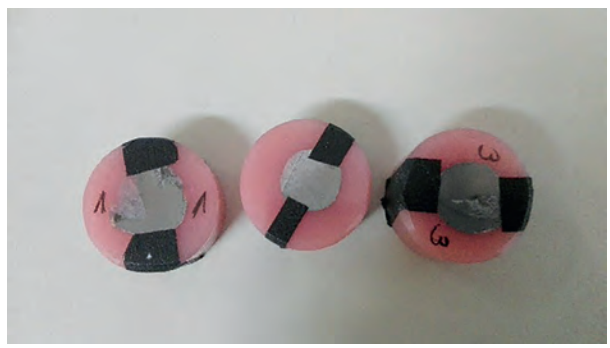

Figure 3.
Lead musket balls prepared for metallographic analysis
Source: Barkóczy–Török 2018.

The two shorter nails with a rectangular cross-section shown on *Figure 1* are 82 mm and 86 mm long. At the points indicated by the arrows, they have a rectangular cross-section measuring 4 × 3 mm. The length of the large nail is 145 mm, and at the place indicated by an arrow it has a rectangular cross-section measuring 8 × 6 mm. The diameters of the lead musket balls are 14 mm, 16 mm, and 17 mm.[5]

[5] The 17 mm lead ball was not discovered in the well, but in one of the supposed siege trenches in 2012. The 17 mm lead ball was involved in the 2018 analyses only as a test sample for "reference".

Figure 4.
The larger nail with the original wooden structural elements after the removal of the wooden peg and nail from the borehole
Source: Barkóczy–Török 2018.

The larger nail held a cylindrical peg with a diameter of 25 mm in place, in a wooden element, which probably belonged to the well house *(Figure 4).*

The primary purpose of the investigations was the metallographic analysis of the material and microstructure of each sample. Additionally, we wanted to find out the possible features of the manufacturing technology of the samples.

As we had the possibility to do destructive material testing, we cut samples from the artefacts for metallographic analyses. *Figures 1–3* show the tested nails in their original state and the samples taken from them. In the case of iron nails, the samples were cut off with a thin bakelite cutting disc, while ensuring that they do not get critically hot. In the case of lead musket balls, which proved to be very soft, we took samples by slow sawing, practically cutting the objects in half *(Figure 3).* Both groups of samples were mechanically abrased and then polished. The lead samples were so soft that particles of the abrasive material stuck into their surface. It was taken into account during the EDS (Energy Dispersive Spectrometer) analyses, and it was not disturbing during the XRF (X-ray Fluorescence Spectroscopy) analyses since the abrased and polished surface was tested. The polished surfaces were etched with a solution of 2 mass percent of natal. In the

case of the lead samples, the steps of polishing and etching were repeated several times, while we tried to remove the easily developing deformed layer. Optical microscopy and mosaic images were taken of the prepared surface using a Zeiss AxioImager microscope at the Institute of Physical Metallurgy, Metal Forming and Nanotechnology, University of Miskolc. Furthermore, scanning electron microscopy (SEM) images were taken and energy-dispersive spectroscopy analyses were carried out using a Hitachi field emission microscope at the Department of Solid State Physics, University of Debrecen. The unpolished surface of the lead balls was also tested with an Oxford Instruments X-MET8000 Expert portable, energy-dispersive X-ray fluorescence (ED-XRF) spectrometer.

The two small nails could be tested freely, whereas in the case of the large nail, we had to keep in mind that the object would be restored later. For this reason, the strategy was to take samples from the head and shank of the small nails across their transversal section, which provided us with sufficient information about the technique of production. Therefore, it was enough to take only a small sample from the tip of the large nail to define the technique of its production.

The mosaic image taken of the head and shank of the small (86 mm long) nail[6] No. 1 is shown by *Figures 5–6*.

The mosaic images well illustrate the layered structure of the nail. It can be seen that layers of different carbon content were forged together forming thus a layered structure. There are several types of fabric structures ranging from completely pearlite-free, coarse, and ferritic areas to layers with ferrite and pearlite. Ferrite is the least carbonaceous element of α-iron (practically 'soft' iron). Pearlite is, on the other hand, a eutectoid of ferrite and cementite (iron carbide, FeC3); it is a harder material of evidently higher carbon content. The sample proved to be very heterogeneous, so we cannot talk about average carbon content. It is striking, however, that we cannot find areas containing significant amounts of carbon, and the proportion of ferrite is high everywhere, over the entire transversal section. The layered structure can be explained by the fact that attempts were made to homogenise the primary raw material (i.e. the iron bloom[7] full of slag inclusions), which was normally heterogeneous in terms of carbon content distribution. This means that the compacted deslagged iron bloom was hammered, folded and forge welded repeatedly – up to 10–15 times – to prepare a primary product (i.e. a thin rod or sheet) to make the subsequent shaping of the desired final product easier. It also occurred that several pieces of iron bloom were forged together and homogenised by multiple folding. However, when the final product – in our case, the iron nail – was prepared, the reheated iron retained its lamellar structure, but the traces of forge welding got blurred and disappeared due to diffusion. In case of objects

[6] The nail at the top in *Figure 2*.

[7] The production of iron bloom was one of the major milestones in the making of iron from its ores. It was an ancient technology going back to the Iron Age. Iron blooms were normally sponge-like blocks with high iron content, which also contained a large amount of slag. They were formed by the smelting of bog iron ores, without their being melted. By hammering, most of the slag could be "pressed" out of this sponge. The contaminated iron bloom was thus forged and compressed. Because the slag had a lower melting point than iron, it practically "got sputtered" from the iron during forging and the iron material completely merged and homogenised. This process was necessary because slag inclusions would have made iron brittle and breakable. The iron blooms were generally not traded, but were processed into semi-finished products in iron forging mills established next to the furnace.

Figure 5.
Mosaic image of the head of the iron nail No. 1
Source: Barkóczy–Török 2018.

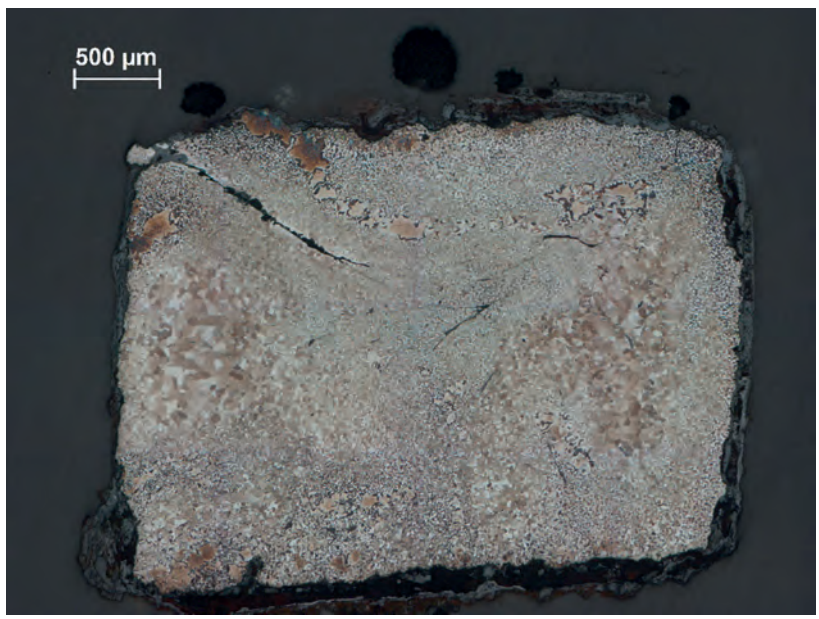

Figure 6.
Mosaic image of a transversal section from the shank of the iron nail No. 1
Source: Barkóczy–Török 2018.

with a thicker cross-section, the traces of forge welding were preserved in the middle of thicker parts, but the layers got thinner towards the surface. Thus, the raw material of the primary product itself is heterogeneous and layered. The nails were made from this raw material with the desired length of shank and cross-section.

It is particularly on the image made of the shank that we can observe an interesting structure, where coarse and fine-grained areas can be seen together. In areas where there is a large amount of pearlite *(Figure 7),* we can observe a structure reverting from partial austenitisation.[8] This suggests hot forging, which is typical when similar objects are made. Of course, partial austenitisation and reverting takes place differently in areas of different carbon content. In ferritic areas its effect is barely noticeable, only the rounded borders indicate it. However, in areas containing ferrite and pearlite, we can see non-austenitised and austenitic structures together, which are identical in terms of quality. It should be borne in mind that the transformation temperature, especially for ferrite particles near pearlite, depends on the carbon content of the immediate volume. For this reason, cooling takes place with different intensity depending on the carbon content. This is why we found regular particles in areas of low carbon content, along with pin-shaped *Widmanstätten* ferrites on the border of areas with high carbon content, containing more pearlite. In terms of fabric structure, the shaping temperature must have been somewhere between 750°C and 800°C, which is the cherry-red level on the colour scale of hot iron, and after the final phase of shaping, the object was cooled in the open air.

Figure 7.
Image taken of the head part (the "shoulder" of the head) of the iron nail No. 1
Source: Barkóczy–Török 2018.

[8] Austenite is a solid solution of iron, the constituents of which are carbon and γ-iron. It is stable at a temperature range from 730°C to 1490°C depending on its carbon content.

The preparation of the nail head is an interesting question. The head, similarly to the shank, has a layered structure. There is much more pearlite on the right side of the shank, and more pearlite can be observed on the same side of the head, as well. The left side of the head is almost completely ferritic, and the shank is likewise. If we regard the running of the layers as a strand orientation, it can be observed that the strand orientation of the shank shows an inclination in the head part due to jumping. It bends backwards to the right where the joining of the head is longer and contains more material. Based on this, we can name jumping as the technology used for shaping the head, which has been a traditional method in nail making for centuries.

The SEM/EDS analysis detected no element other than iron and carbon in the material of the nail *(Table 1).* The material structure contained relatively few inclusions extended in the direction of formation *(Figure 8).* The results of EDS analyses in *Tables 2 and 3* show that the inclusions have very high iron oxide content. Fayalite ($2FeO\ SiO_2$), which is common in iron smelting slags, is apparently not dominant here. These inclusions reflect the general composition of typically Ca–Fe silicate smithing slags with a significant wüstite phase (FeO). The relatively small amounts of aluminium, magnesium and potassium are probably components of complex oxides.

Table 1.

The element composition of the base material of the iron nail No. 1

Element	C weight [wt.%]	C atom [at.%]
C 6	0.59	2.61
O 8	1.15	3.82
Fe 26	98.26	93.56
Total	**100.00**	**100.00**

Source: Barkóczy–Török 2018.

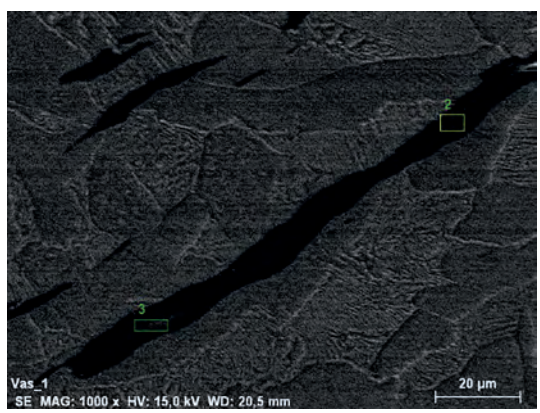

Figure 8.

SEM/EDS analysis of the long (elongated) inclusions (labelled with numbers 2 and 3) in the iron nail No. 1

Source: Barkóczy–Török 2018.

Table 2.
The analysis of area 2 in the selected inclusion of the iron nail No. 1

Element	C weight [wt.%]	C atom [at.%]
C 6	0.06	0.19
O 8	10.40	24.31
Mg 12	3.68	5.66
Al 13	3.32	4.60
Si 14	10.24	13.63
K 19	1.09	1.04
Ca 20	10.99	10.25
Fe 26	60.22	40.31
Total	**100.00**	**100.00**

Source: Barkóczy–Török 2018.

Table 3.
The analysis of area 3 in the selected inclusion of the iron nail No. 1

Element	C weight [wt.%]	C atom [at.%]
C 6	0.23	0.74
O 8	9.80	23.55
Mg 12	2.83	4.48
Al 13	2.47	3.52
Si 14	9.30	12.74
K 19	0.62	0.61
Ca 20	10.55	10.12
Fe 26	64.21	44.23
Total	**100.00**	**100.00**

Source: Barkóczy–Török 2018.

In the following, we will analyse similarities to and deviations from the above-mentioned properties of nail No. 1 in nails No. 2 and No. 3. The analysis of the head part of – the 82 mm long – nail No. 2 (i.e. the nail in the middle in *Figure 2*) revealed an even more characteristic layered structure and a specific texture, which developed due to the homogenisation of the primary product *(Figures 9–10).* At some places, there is an extensive diffusion zone between the layers with low and high pearlite content, while at other places, this layer is quite thin. The large diffusion zone is caused by the carbon diffusion that developed in the iron bloom, whereas the narrow diffusion zone goes back to the diffusion that developed at the boundaries of the homogenising fold in the heat of forging. In this nail, we also found evidence that the forging was carried out only in a semi-austenitised state *(Figure 11).* Furthermore, we could again observe areas rich in ferrite and pearlite, suggestive of free cooling.

The texture of nail No. 2 clearly demonstrates that the nail head was formed by jumping the material of the nail itself. In this nail, we could also find completely pearlitic areas, which could not be observed in the previous case. The microstructure is heterogeneous here, as well.

Therefore, it is not worth determining the average carbon content. The SEM/EDS analysis *(Figure 12 and Table 4)* did not show significant contamination in this nail either; in fact, it is an almost pure iron-carbon alloy. The two nails are significantly similar to each other in terms of the manufacturing technology and the basic microstructural properties of the material.

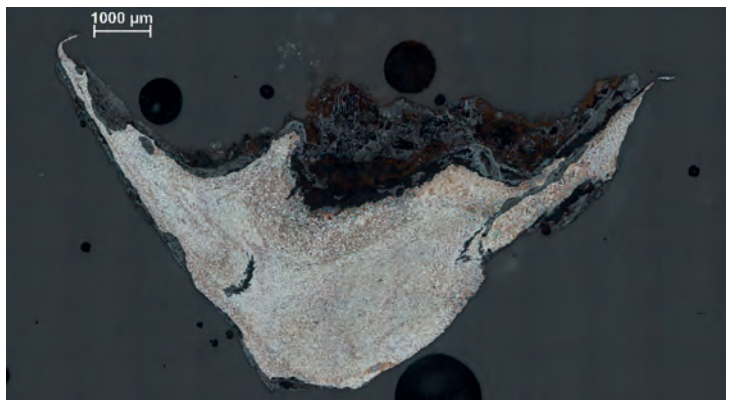

Figure 9.
Mosaic image of the head part of the iron nail No. 2
Source: Barkóczy–Török 2018.

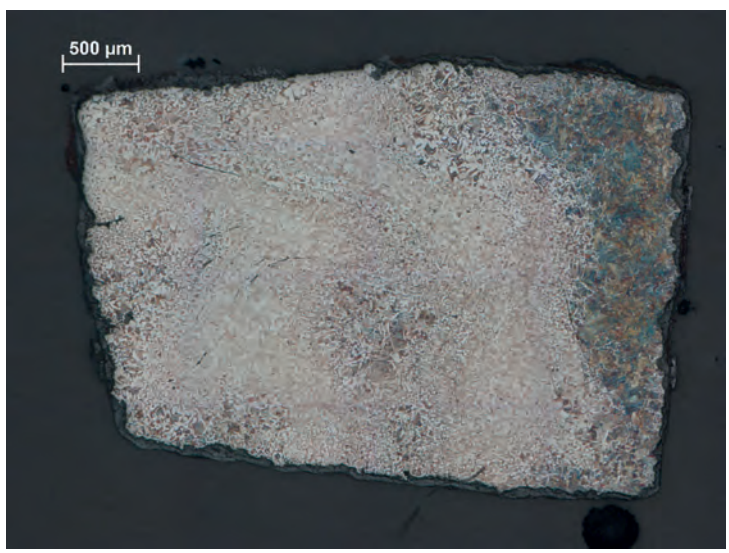

Figure 10.
Mosaic image of the transversal section from the shank of the iron nail No. 2
Source: Barkóczy–Török 2018.

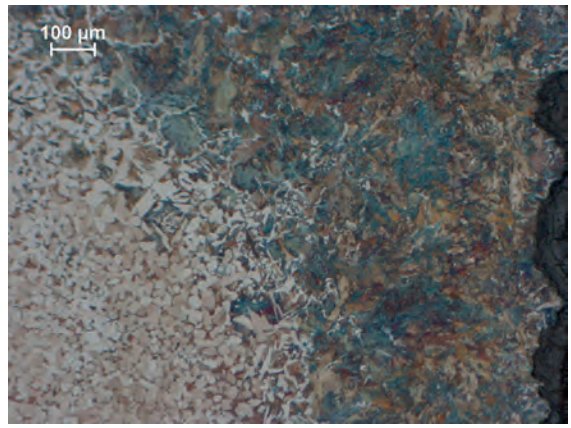

Figure 11.
Image of the transversal section from the shank of the iron nail No. 2
Source: Barkóczy–Török 2018.

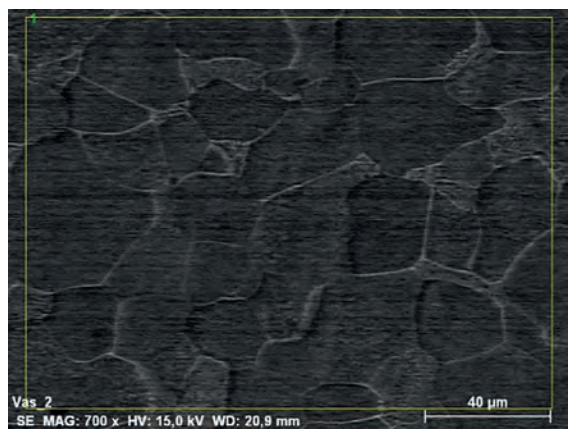

Figure 12.
The composition analysis of the base material of the iron nail No. 2
Source: Barkóczy–Török 2018.

Table 4.
The element composition of the base material of the iron nail No. 2

Element	C eight [wt.%]	C atom [at.%]
C 6	0.62	2.8
Fe 26	99.38	97.2
Total	**100.00**	**100.00**

Source: Barkóczy–Török 2018.

Elongated inclusions also appeared in the tissue of the iron nail No. 2 in the direction of shaping, but smaller, spherical (i.e. undistorted) inclusions can also be observed. The microstructure revealed by the etching of one of the examined inclusions clearly shows two phases. Both areas were subjected to SEM/EDS analyses *(Figure 13 and Tables 5–7).* The light phase consists mainly of iron oxide. The dark phase around it has a composition similar to that of the iron nail No. 1, except that it has a higher silicon content and less calcium can be measured in it. This inclusion can also be regarded as a remnant of a smithing slag, as it is suggested by the high iron oxide content. The unique use of the former blacksmithing additive may also contribute to the change in the basicity of the slag inclusions (CaO/SiO_2), that is, to a certain degree of heterogeneity between the inclusions.

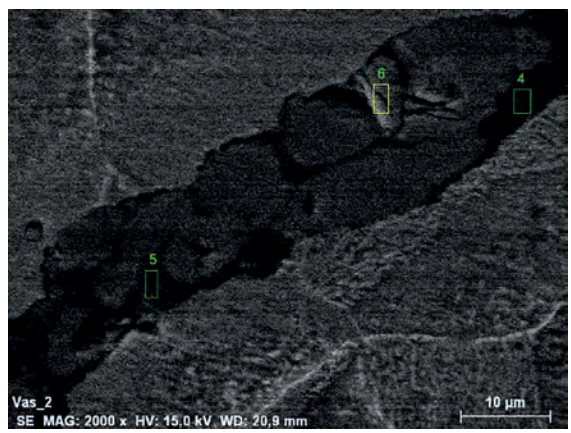

Figure 13.

SEM/EDS analysis of the long (elongated) inclusions (labelled with numbers 4–6) in the iron nail No. 2

Source: Barkóczy–Török 2018.

Table 5.

The analysis of area 4 in the selected inclusion of the iron nail No. 2

Element	C weight [wt.%]	C atom [at.%]
C 6	0.13	0.36
O 8	19.57	38.88
Al 13	5.03	5.92
Si 14	16.64	18.60
P 15	0.98	1.00
K 19	5.12	4.16
Ca 20	4.65	3.69
Mn 25	2.30	1.33
Fe 26	45.77	26.05
Total	**100.00**	**100.00**

Source: Barkóczy–Török 2018.

Table 6.

The analysis of area 5 in the selected inclusion of the iron nail No. 2

Element	C weight [wt.%]	C atom [at.%]
C 6	0.29	0.68
O 8	26.71	47.88
Mg 12	0.94	1.11
Al 13	5.21	5.54
Si 14	16.15	16.49
P 15	0.77	0.71
K 19	4.54	3.33
Ca 20	4.60	3.29
Mn 25	1.63	0.85
Fe 26	39.16	20.11
Total	**100.00**	**100.00**

Source: Barkóczy–Török 2018.

Table 7.

The analysis of area 6 in the selected inclusion of the iron nail No. 2

Element	C weight [wt.%]	C atom [at.%]
C 6	1.12	3.35
O 8	20.81	46.58
Fe 26	78.07	50.06
Total	**100.00**	**100.00**

Source: Barkóczy–Török 2018.

According to the testing strategy, the smallest sample was taken from the large nail (the nail at the bottom in *Figure 2*) with great care. In this case, our experience gained from the former analysis of the two shorter nails was fundamentally used for comparison. Only a transversal sample was taken from the end of the shank, close to the tip of the nail, so that it could be restored easily. This, of course, also means that the sample is not representative in all respects, but it still adequately reflects the properties relevant to our study. In the mosaic image of the large nail *(Figure 14),* large-grained ferrite can be seen over a significant part of the transversal section, which is suggestive of low carbon content. The lower part of the transversal section shows a layer of large carbon content, which is similar to the nails described above. On the right side of the transversal section, one can see elongated particles, the longitudinal axis of which is parallel to the given side. This indicates a moderately warm or possibly cold shaping. The elongated shape of the particles presumably developed when the nail was made, but it cannot be ruled out either that it was formed when the object was in use, already in a cold state. On the right of the transversal section, there is a cavity containing a series of inclusions, which may have evolved during the manufacturing process and it testifies to the relatively rapid, simple and not very thorough forging of a simple product, which is likely to have been produced in large numbers. It is certain that the technology of production was the same as in the case of the other two nails above. The SEM/EDS analysis shows in this case again a pure iron-carbon alloy without other alloying agents, in which the quantity of impurities is insignificant *(Table 8).*

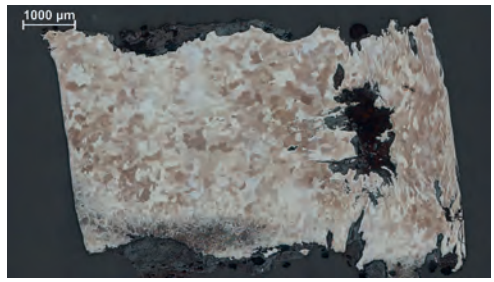

Figure 14.
Mosaic image of the transversal section of the iron nail No. 3
Source: Barkóczy–Török 2018.

Table 8.
The element composition of the base material of the large iron nail

Element	C weight [wt.%]	C atom [at.%]
C 6	0.46	2.10
Fe 26	99.54	97.90
Total	**100.00**	**100.00**

Source: Barkóczy–Török 2018.

In the examined transversal section of the large nail, we could find inclusions mainly near the cavity. The results of the analyses are shown in *Figure 15 and Tables 9–11.* The EDS results of the inclusion test show a much lower iron content compared to the compositions of the two smaller nails discussed above. Nevertheless, the Si content is slightly higher, and the Ca content is also high. The relatively high CaO/SiO_2 basicity reflected by the results of the EDS analysis does not indicate inclusions of iron smelting slags. These are probably also the remains of smithing slags, which contain a higher proportion of slag-forming and fluxing material.

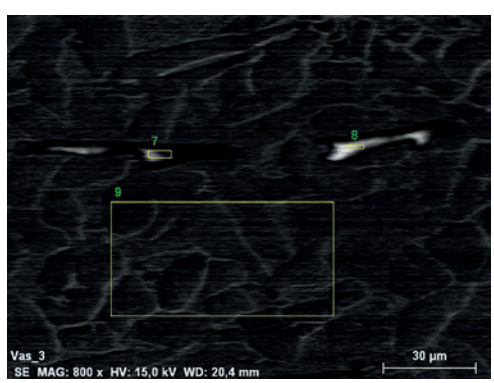

Figure 15.
SEM/EDS analysis of the long (elongated) inclusions (labelled with numbers 7–9) in the large iron nail
Source: Barkóczy–Török 2018.

Table 9.

The analysis of area 7 in the selected inclusion of the large iron nail

Element	C weight [wt.%]	C atom [at.%]
C 6	0.01	0.02
O 8	28.60	50.12
Mg 12	1.58	1.82
Al 13	3.62	3.76
Si 14	14.44	14.42
P 15	0.54	0.49
K 19	3.59	2.57
Ca 20	14.40	10.08
Mn 25	3.84	1.96
Fe 26	29.38	14.75
Total	**100.00**	**100.00**

Source: Barkóczy–Török 2018.

Table 10.

The analysis of area 8 in the selected inclusion of the large iron nail

Element	C weight [wt.%]	C atom [at.%]
C 6	0.83	1.92
O 8	28.03	48.55
Mg 12	2.57	2.93
Al 13	2.67	2.74
Si 14	14.84	14.64
P 15	0.53	0.48
K 19	2.88	2.04
Ca 20	15.47	10.70
Mn 25	4.12	2.08
Fe 26	28.06	13.92
Total	**100.00**	**100.00**

Source: Barkóczy–Török 2018.

Table 11.

The analysis of area 9 in the selected inclusion of the large iron nail

Element	C weight [wt.%]	C atom [at.%]
C 6	0.97	4.34
Fe 26	99.03	95.66
Total	**100.00**	**100.00**

Source: Barkóczy–Török 2018.

Overall, the nails were wrought by warm and semi-warm forging. Due to the heterogeneous structure of the iron bloom, heterogeneity can also be observed in the material structure of the objects, even after homogenisation. The most prominent features of the inclusions are the high iron oxide and Ca contents. The inclusions are basically remnants of by-products that developed during pre-forging and shaping.

The production technique of the three nails is the same, and their base material was also prepared with very similar care. Based on the material analyses, the production technique can be connected to contemporary work methods depicted in *Figures 16 and 17.*

A German image from 1482[9] *(Figure 16, on the left)* shows the nailer sitting on a stool and working with a hammer on a nail glowing red. The nailsmith jumps the head of a nail fitting it into a special punched tool used for forming nails. *Figure 16, on the right* (a German depiction from 1525) depicts the same process, but in this case, the background represents not only the built smithing hearth together with the primary products, but the bellow used for the smithing hearth can also be well observed. The nail depicted by the image on the left is very similar to the big iron nail investigated by us from the aspect of the shaping of the head. The image also demonstrates that this shaping of the nail heads was employed as early as the seventeenth century.

Figure 16.

Nailsmiths during work

Source: image on the left: www.nuernberger-hausbuecher.de/75-Amb-2-317-101-r (Accessed: 20 April 2019.); image on the right: www.nuernberger-hausbuecher.de/75-Amb-2-317-140-v/data (Accessed: 20 April 2019.)

[9] The source (www.nuernberger-hausbuecher.de/75-Amb-2-317-101-r) also connects this representation to a work dated to 1522.

In a third German image, dated to 1572 *(Figure 17),* the nailer is in his workshop, sitting on a work block designed for this purpose. He hammers a nail from the tip of a long iron rod on an anvil. Because of the size of the product, right next to the small anvil, there is a wedge-shaped cutter ready to be used. The smith could cut off the finished tip with it. The flames in the free-standing fireplace behind him are fanned by his assistant. The finished wrought nails are stored in two 'selling bowls', and the range of products are displayed next to it.

Figure 17.

Nailer in his workshop (a German image from 1572)

Source: www.nuernberger-hausbuecher.de/75-Amb-2-317b-28-v/data (Accessed: 20 April 2019.)

In the case of lead musket balls, the exploration of the microstructure proved to be rather difficult, because lead is a very soft material, and this rendered the mechanical preparation for analysis very troublesome. Only after several cycles of polishing and etching were we able to obtain a microstructure suitable for analysis *(Figure 18).* It was noticeable that the preparation of lead balls with a small diameter was more difficult, probably because they were made of an even softer material than the large balls. The dendrite arms can be observed in the microstructure. The secondary dendrite arm spacing is approximately 10μm, which is indicative of rapid cooling. This may be due to the use of an iron/steel mould for the balls. The polyhedron black phases in the microstructure are Si-carbide particles originating from the preparation of objects for analysis, which unfortunately easily

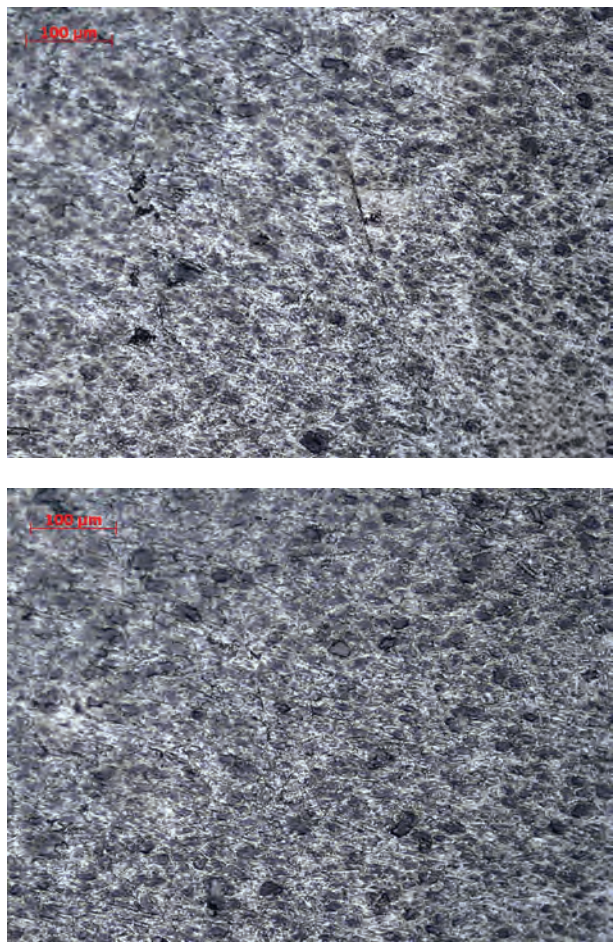

Figure 18.
Microstructure of the 16 mm (above) and the 17 mm (below) musket balls
Source: Barkóczy–Török 2018.

get stuck into the soft surface and slightly disturb the analysis. The samples clearly show the properties of casting, and the parting plane may also be well observed. We cut the balls perpendicular to the parting plane.

The SEM/EDS analysis showed that all the balls were cast from unalloyed lead. However, the 16 mm and 17 mm balls contained phases with high nickel and low phosphorus contents *(Figure 20 and Table 13).* These were clearly caused by contamination and made the composition of the lead balls slightly solider. Nickel and lead form a monotectic system, i.e. these phases get enriched and push crystallisation to a lower temperature. The 14 mm ball is made of virtually pure lead *(Figure 21 and Table 14),* with no impurities detected by the EDS analysis.

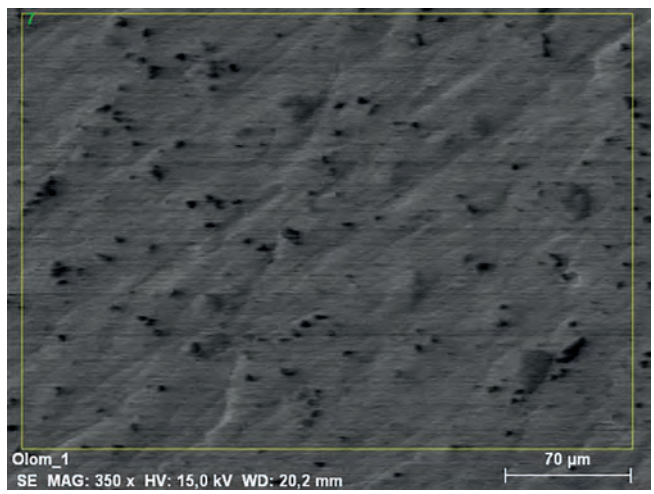

Figure 19.

Analysis of the average composition of the 16 mm lead musket ball

Source: Barkóczy–Török 2018.

Table 12.

Analysis of the average composition of the 16 mm lead musket ball

Element	C weight [wt.%]	C atom [at.%]
C 6	9.46	48.77
O 8	6.77	26.19
Pb 82	83.78	25.04
Total	**100.00**	**100.00**

Source: Barkóczy–Török 2018.

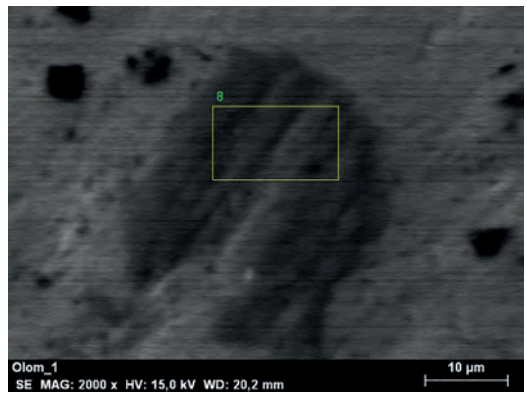

Figure 20.
Analysis of the nickel-rich phase of the 16 mm lead musket ball
Source: Barkóczy–Török 2018.

Table 13.
Analysis of the nickel-rich phase of the 16 mm lead musket ball

Element	C weight [wt.%]	C atom [at.%]
C 6	0.87	4.13
O 8	2.02	7.18
P 15	6.87	12.62
Ni 28	73.81	71.55
Pb 82	16.43	4.51
Total	**100.00**	**100.00**

Source: Barkóczy–Török 2018.

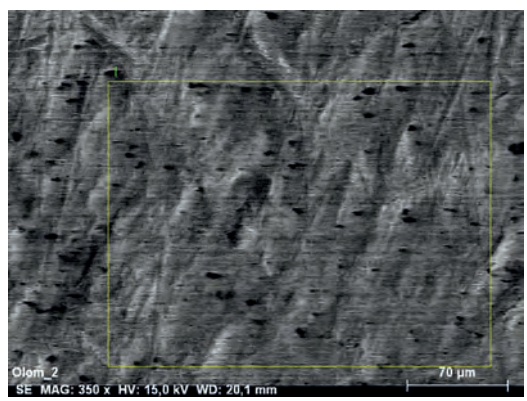

Figure 21.
Analysis of the average composition of the small, 14 mm lead musket ball
Source: Barkóczy–Török 2018.

Table 14.

Analysis of the average composition of the small, 14 mm lead musket ball

Element	C weight [wt.%]	C atom [at.%]
C 6	7.95	47.82
O 8	4.81	21.74
Pb 82	87.24	30.44
Total	**100.00**	**100.00**

Source: Barkóczy–Török 2018.

The results of the XRF tests of the unpolished halves of the lead balls cut in half are shown in *Table 15.* Nickel impurities do not appear here – the uncontaminated parts of the surface were placed under the XRF spectrometer. The indicated palladium and iridium contents are probably the result of peak overlapping caused by over-excitation and do not signal real presence of the mentioned elements. Lead is relatively difficult to excite, but this test also confirms that the balls consist of pure lead.

Table 15.

The results of the XRF analysis of the lead musket balls expressed in weight percent

Sample	Testing time (s)	Pb	Fe	Ag	Pd	Ir
Lead ball1 1	30	**98.60**	0.21	0.10	0.27	0.61
Lead ball1 2	30	**98.49**	0.27	0.07	0.33	0.61
Lead ball1 3	30	**98.67**	0.21	0.10	0.29	0.53
Lead ball2 1	30	**98.80**	0.07	0.09	0.29	0.56
Lead ball2 2	30	**98.82**	0.09	0.11	0.32	0.46
Lead ball2 3	30	**98.88**	0.07	0.09	0.31	0.43
Lead ball3 1	30	**98.43**	0.16	0.11	0.33	0.64
Lead ball3 2	30	**98.32**	0.18	0.08	0.30	0.59
Lead ball3 3	30	**98.06**	0.56	0.10	0.36	0.65

Note: The lead balls in the table are indicated as follows: Lead ball1 = 16 mm, Lead ball2 = 14 mm, Lead ball3 = 17 mm.

Source: compiled by the author

The xylotomic[10] analysis[11] of wood material discovered in the well at Zrínyi-Újvár during the archaeological investigation

Three pieces from a structural element of the well were selected for scientific xylotomic tests of wood material uncovered from the well of the Zrínyi-Újvár archaeological site. During the study of wood material, we were positive that the identification of a given species would contribute to our knowledge of plant-based raw materials and their use in a certain period, as well as to a better understanding of vegetation and, thus, the wider environment, as well.

The three tested structural elements are presumably wood materials preserved to varying degrees in partially wet and dry conditions. The samples taken from charred wood were relatively poorly preserved, whereas the preservation of samples taken from uncharred wood was considered good.

At first, we took samples from the selected wood elements using a chainsaw. Next, the transverse surface suitable for testing was formed with a belt sander and by hand sanding. The tree anatomy was studied with a stereo microscope. To measure the widths of tree rings, the samples were scanned at 1,200 dpi resolution using a calibration slide. The scanned images were processed with the QGIS 3.2.0 'Bonn' software. The actual width of the tree rings measured in the program was determined on the basis of ratios – in the knowledge of 1 mm on the calibration slide – with an accuracy of 1/1,000 mm. The conversion of the data obtained this way were converted into Heidelberg format using the TRiCYCLE 0.3.1 Dendro Data Converter program, and the lists of data were displayed with the MS Excel and Tellervo 1.0 programs.

To display the vegetation of the site – and its close surroundings – we made images with the QGIS 3.2.0 'Bonn' program, using the following sources:

- Marosi S. – Somogyi S.: Magyarország kistájainak katasztere [Inventory of Microregions in Hungary]. 1990.
- Zólyomi B.: Természetes növénytakaró [Natural Vegetation]. 1989.
- SRTM 90 m Digital Elevation Data – *Jarvis et al.* 2008.
- Első katonai felmérés [First Military Survey] – Map Collection of the Ministry of Defence, Institute and Museum of Military History, map sheets IV/17 and V/23, 1784, in 1:28,800 scale, digital edition by Arcanum 2004.
- Második katonai felmérés [Second Military Survey] – Map Collection of the Ministry of Defence, Institute and Museum of Military History, map sheets XXIII/61 and XXIV/61, 1858–1859, in 1:28,800 scale, digital edition by *Tímár et al.* 2006.
- Harmadik katonai felmérés [Third Military Survey] – Map Collection of the Ministry of Defence, Institute and Museum of Military History, map sheet 5458/3, 1879, in 1:25,000 scale, digital edition by *Biszak et al.* 2007.

[10] Xylotomic analysis is aimed at the examination of tissues from ligneous plant remains to determine tree species.

[11] The examinations and evaluation of the results were carried out by Dr. Dénes Saláta, Associate Professor at the Department of Nature Conservation and Landscape Ecology, Faculty of Agriculture and Environmental Sciences, Institute of Nature Conservation and Landscape Management, Szent István University. *Saláta* 2018.

- Topográfiai térképek a II. világháború idejéből [Topographic Maps Used in World War II] – Map Collection of the Ministry of Defence, Institute and Museum of Military History, map sheet 5458/NY, 1940–1944, in 1:50,000 scale, digital edition by *Tímár et al.* 2008.

Each of the preserved samples charred in varying degrees belong to a deciduous tree (to ring-porous deciduous trees) in terms of wood anatomy.[12] With regard to the species, it can be determined that the samples belong to the oak species. Based on the large vessels found in several rows in the broad earlywood rings and the latewood vessels forming gradually narrowing, forked radial rows,[13] they presumably come from a sessile oak *(Quercus petraea)* – division of angiosperms *(Angiospermatophyta),* class of dicotyledons *(Dicotyledonopsida),* order of beeches *(Fagales),* family of beeches *(Fagales),* genus *Quercus.*[14]

It must be noted here that – according to the current international state of tree anatomy – pedunculate, sessile and pubescent oak species cannot be differentiated exclusively on the basis of their wood anatomy[15] *(Figure 22),* although some works[16] may help us do it within certain limits.

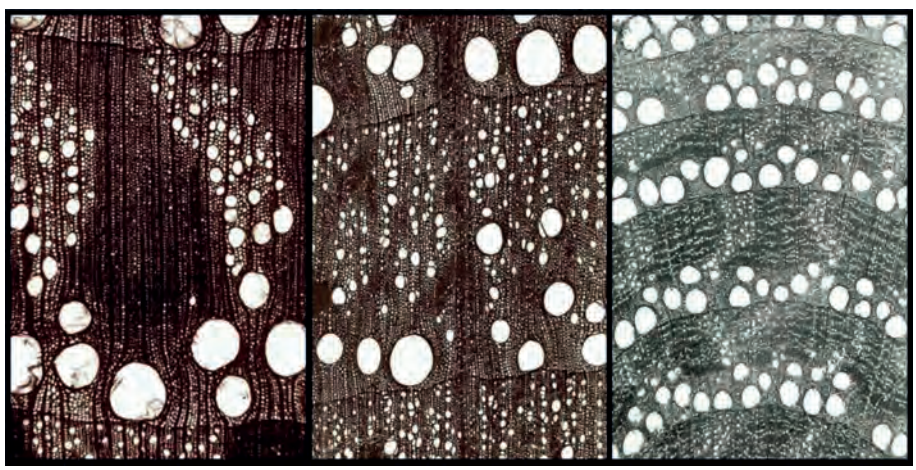

Figure 22.
Microscopic image of the transversal section of pedunculate, sessile and pubescent oak trees
Source: Schoch et al. 2004. www.woodanatomy.ch (Accessed: 20 April 2019.)

The wood sample is in a good, in fact, excellent condition. It is dry, and a part of it is slightly charred due to fire *(Figure 23).* The wood material is presumably a structural element of

12 *Babos* 1994; *Molnár–Peszlen–Paukó* 2007.
13 *Babos* 1994.
14 *Simon* 2000.
15 *Schweingruber* 1990; *Schoch–Heller–Schweingruber–Kienast* 2004.
16 *Greguss* 1959; *Babos* 1994 or *Molnár–Peszlen–Paukó* 2007.

the well lining, comprising a wooden peg on one side necessary for joining. The burn mark suggests that the sample was exposed to fire for a short period of time – at least, in comparison with Samples 2 and 3.

Having studied the transversal section of the sample *(Figure 24),* we can conclude that the piece of wood comes from a ring-porous deciduous tree, most probably a sessile oak (v. sim.[17] *Quercus petraea*), and also that it was formed from the tree trunk.

Figure 23.
Sample 1 found in the well of the Zrínyi-Újvár archaeological site
Source: Saláta 2018.

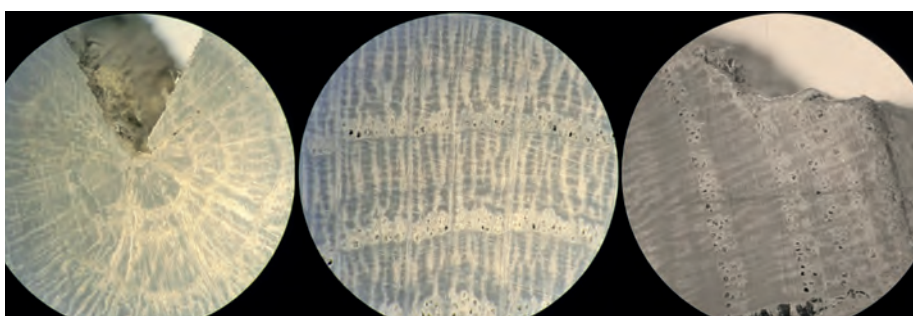

Figure 24.
Microscopic images of the characteristic transversal sections of Sample 1 found in the well of the Zrínyi-Újvár archaeological site
Source: Saláta 2018.

[17] Veri simile.

The growth trend of the sample *(Figures 25 and 26)* shows that the tree grew rather unevenly in the first 10 to 12 years. In the following 20 years, the tree grew relatively significantly, apart from a 4-year period of modest growth. Subsequently, around years 30–32 a generally declining growth trend with relatively narrow, densely spaced annual rings started. The annual rings of earlywood from years 10 to 30 are quite wide (6–8 mm), so it is likely that the tree came from a habitat with favourable conditions. Furthermore, based on the image of the heartwood and the annual rings, the structural element was made from the trunk of the felled tree.

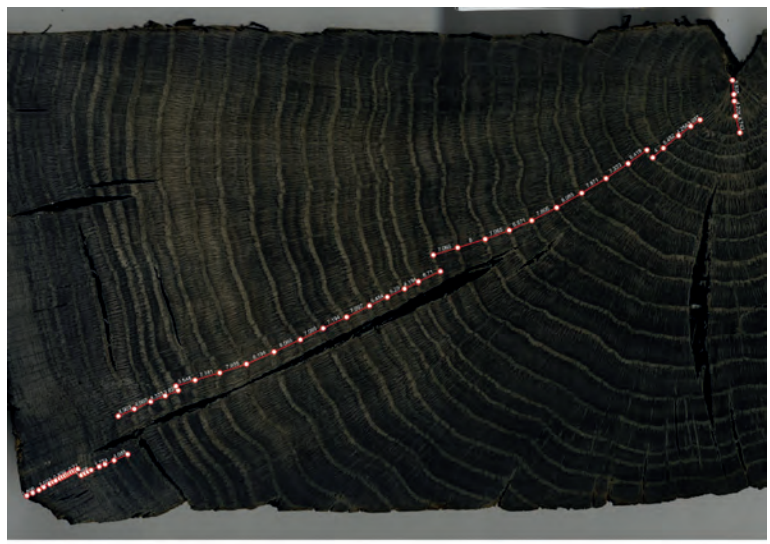

Figure 25.
Transversal section of Sample 1 discovered in the well of the Zrínyi-Újvár archaeological site displaying the widths [mm] of the annual rings, made with the QGIS 3.2.0 'Bonn' programme
Source: Saláta 2018.

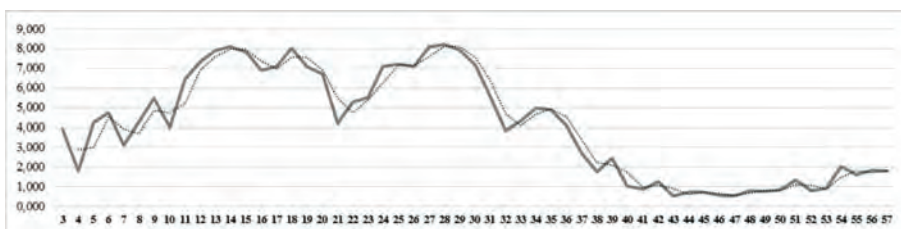

Figure 26.
Annual ring widths [mm] of Sample 1 from the well of the Zrínyi-Újvár archaeological site (continuous line), together with a two-period trendline (dashed line)
Source: Saláta 2018.

The wood sample is in good condition, dry, and its surface is charred due to fire *(Figure 27).* The wood material could have formed the well lining or even the structure of the well house. There is a carved, wrought part in the middle of the piece of wood, which probably served joining. Although the wood was considerably affected by fire, the supposed traces of carving can be seen well at both ends. It can be conferred from the burn mark that the wood was exposed to fire for a long period of time – at least, compared to Sample 1.

After studying the transversal section of the sample *(Figure 28),* we can conclude that the piece of wood belongs to a ring-porous deciduous tree, most probably a sessile oak (v. sim. *Quercus petraea*), and also that it was cut from the tree trunk.

The microscopic image of the transversal section of the sample has revealed several details that are worth being emphasised here. The left side of *Figure 29* shows a fragment of the annular rings preserved in a dry state. It is clearly visible that the large vessels of the earlywood form several rows. The image in the middle illustrates the effect of carbonisation on wood. The image on the right shows a ring-porous xylem with a few and narrow annual rings that developed in early spring, which was probably the result of some kind

Figure 27.
Sample 2 from the Zrínyi-Újvár archaeological site
Source: Saláta 2018.

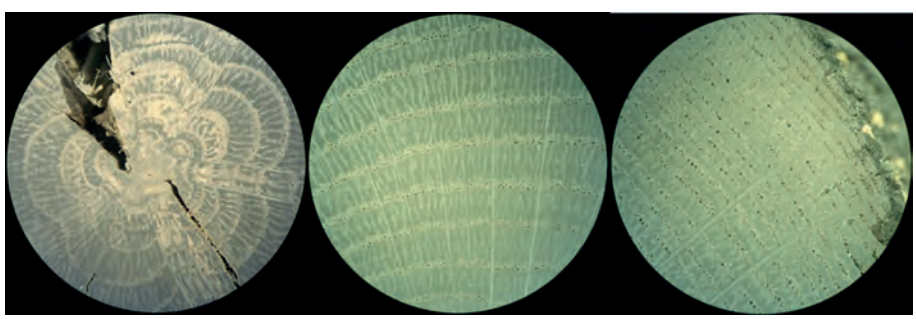

Figure 28.
Microscopic images of the characteristic transversal sections of Sample 2 found in the well of the Zrínyi-Újvár archaeological site
Source: Saláta 2018.

of deformation resulting in the transformation of the wood tissue. The recorded growth trend *(Figures 30 and 31)* demonstrates that the tree grew relatively hectically during its first 18–20 years, which was followed by a generally declining trend. Special mention must be made of the slow-growing phase in years 22–25, which is also clearly visible in the transversal section (in the middle of *Figure 30*). The annual rings of the early growth phase and those of latewood are quite wide, so the tree probably comes from a habitat with favourable conditions. Based on the image of the heartwood and the annual rings, the structural element was made from the trunk of the felled tree.

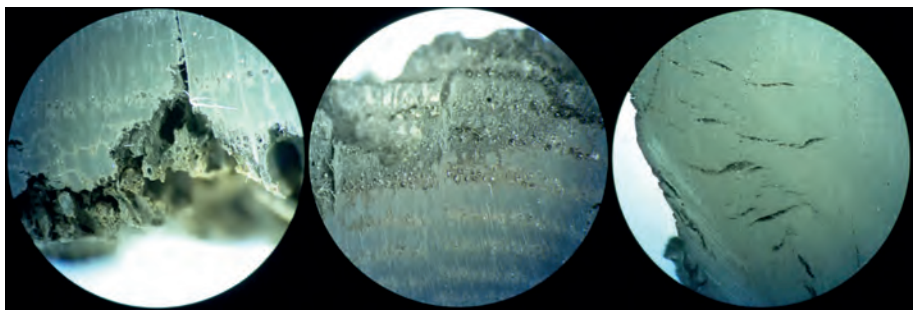

Figure 29.
Details of the transversal sections of Sample 2 found in the well of the Zrínyi-Újvár archaeological site observed under a microscope, which are worth being highlighted
Source: Saláta 2018.

Figure 30.
Transversal section of Sample 2 discovered in the well of the Zrínyi-Újvár archaeological site displaying the widths [mm] of the annual rings, made with the QGIS 3.2.0 'Bonn' programme
Source: Saláta 2018.

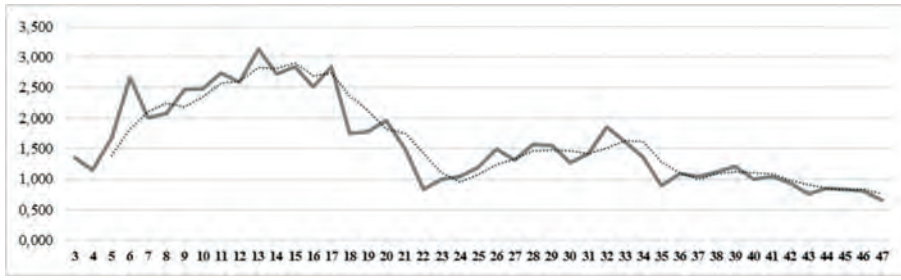

Figure 31.
Annual ring widths [mm] of Sample 2 from the well of the Zrínyi-Újvár archaeological site (continuous line), together with a two-period trendline (dashed line)

Source: Saláta 2018.

The sample is relatively well-preserved, dry, charred on the surface due to fire, and covered with clay loam and sand sediments *(Figure 32).* The wood was probably a structural element of the well lining or the well house, and although it was considerably affected by fire, it clearly shows the signs of carving on both ends. It can be inferred from the burn mark that the wood – at least, when compared to Samples 1 and 2 – was exposed to the effect of fire for a long period of time.

Having studied the transversal section of the sample *(Figure 28),* we can conclude that the piece of wood belongs to a ring-porous deciduous tree, most probably a sessile oak (v. sim. *Quercus petraea*), and also that it was cut from the tree trunk.

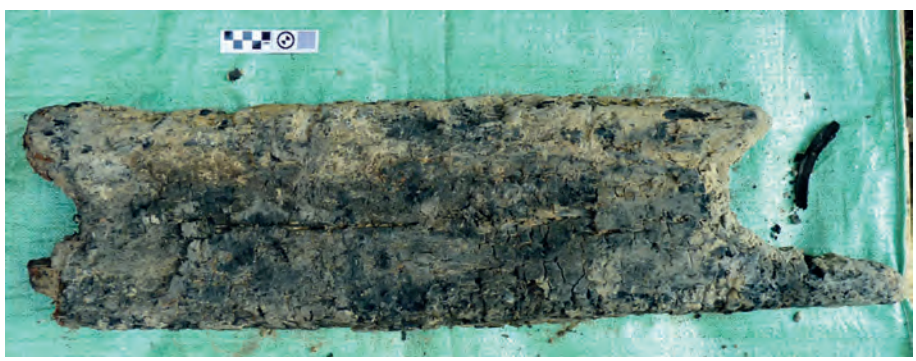

Figure 32.
Sample 3 from the Zrínyi-Újvár archaeological site

Source: Saláta 2018.

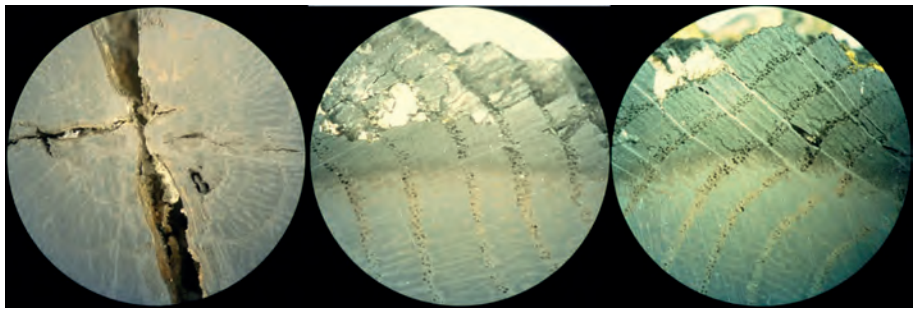

Figure 33.
Microscopic images of the characteristic transversal sections of Sample 3 found in the well of the Zrínyi-Újvár archaeological site
Source: Saláta 2018.

After studying the transversal section of the sample under a microscope, there are several details worth being emphasised. *Figure 33* shows the effect of carbonisation on wood, while *Figure 34* represents the passage caused by a pest. Its diameter is approximately 1–2 mm, so it is likely to be the woodworm hole and burrow of a common furniture beetle.[18]

The recorded growth trend *(Figures 35 and 36)* reveals that the tree grew relatively hectically in its first 18–20 years, which was presumably followed by a declining growth. However, due to the burn, we have information only about approximately 30 years. The annual rings and the latewood are quite wide, so the tree probably came from a habitat with favourable conditions. Based on the image of the heartwood and the annual rings, the structural element was made of the trunk of the felled tree.

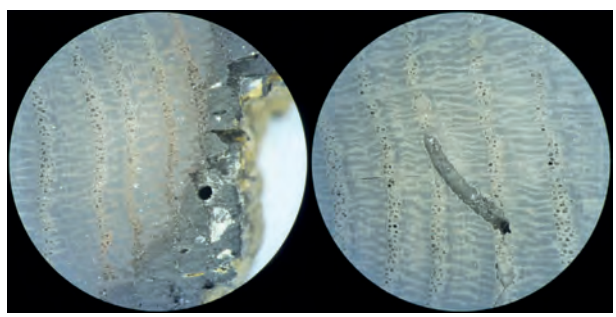

Figure 34.
Details of the transversal sections of Sample 3 found in the well of the Zrínyi-Újvár archaeological site observed under a microscope, which are worth being highlighted
Source: Saláta 2018.

[18] The habitats of the death watch beetle *(Xestobium rufovillosum Deg.)* and the common furniture beetle *(Anobium pertinax L.)* are equally connected to oak trees. – Family *Anobiidae* in *Brehm's* Life of Animals.

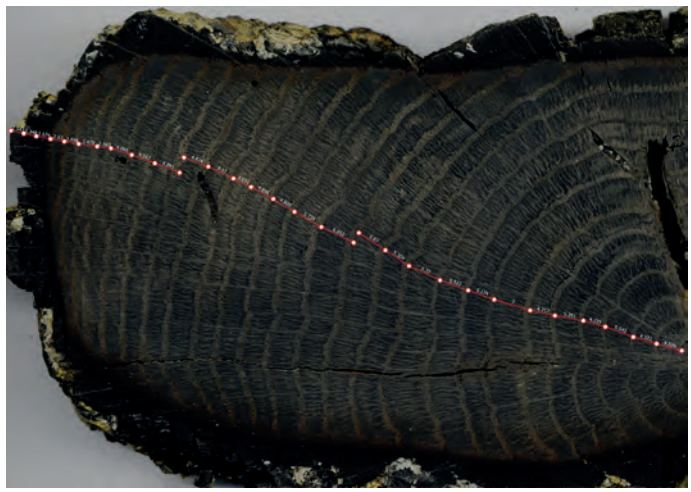

Figure 35.
Transversal section of Sample 3 discovered in the well of the Zrínyi-Újvár archaeological site displaying the widths [mm] of the annual rings, made with the QGIS 3.2.0 'Bonn' programme
Source: Saláta 2018.

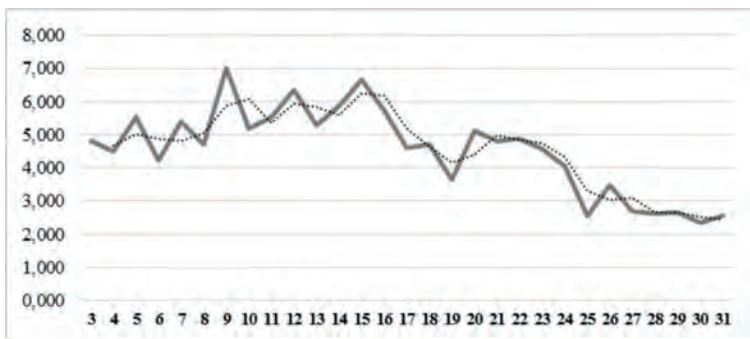

Figure 36.
Annual ring widths [mm] of Sample 3 from the well of the Zrínyi-Újvár archaeological site (continuous line), together with a two-period trendline (dashed line)
Source: Saláta 2018.

The investigated pieces of wood discovered in the archaeological site are highly likely to belong to the drought-tolerant sessile oak species. Based on the site, they can be dated to the seventeenth century, which period – in terms of climate and vegetation change – belongs to the Subatlantic climate period, or beech phase 2.[19]

[19] *Járainé* 2006.

We are in the same phase today, so the map[20] by Bálint Zólyomi representing the possible natural vegetation is extremely relevant and important for the question of vegetation in the examined area *(Figure 37).* It should be noted, however, that due to human activity, the vegetation cover may have significantly changed since the seventeenth century. The natural vegetation of the mountains consisted (and still consists) of oak forests, mixed hornbeam and oak forests and beech forests, while the characteristic flora of the Great Plain was the oak forest steppe.[21]

The investigated area is located on the border of the micro-regions Zalaapáti-hát ('Zalaapáti High Plains') and Mura-balparti sík ('Plains on the Left Bank of the Mura'), in the meso-region of Zalai-dombság ('Zala Hills') belonging to the West Hungarian Border Region. The whole of the former micro-region is a potential forest area with hornbeam trees, and secondarily with shrub-sessile oak trees in its lower parts. The vegetation of the latter micro-region is varied, and it has groves consisting of oak, ash, and elm trees on its more elevated parts.

The map by Zólyomi indicates that the close surroundings of the site must have had floodplain grove forests, mixed Illyrian hornbeam and oak forests, Balkanic Turkey oak and sessile oak forests, sand oak forests, as well as Illyrian beech forests.

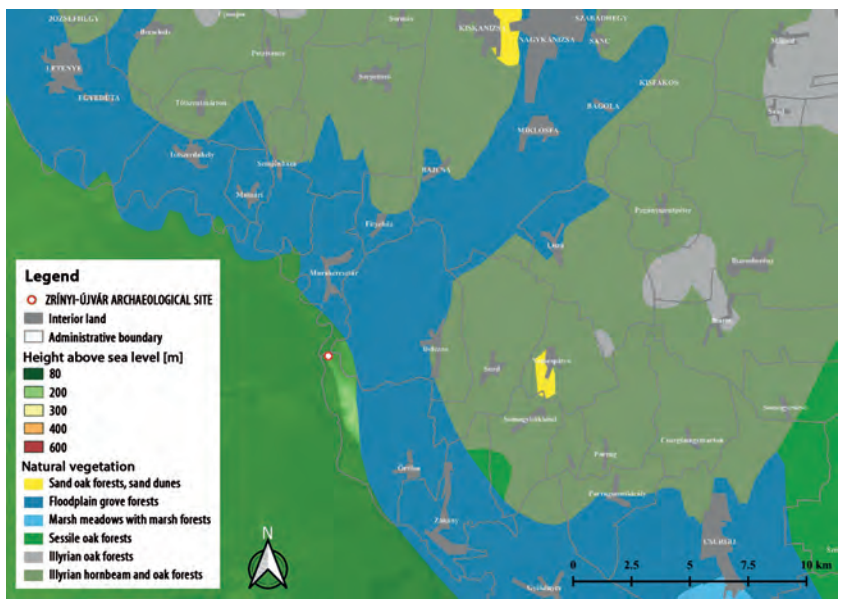

Figure 37.

Natural vegetation in the wider environment of the archaeological site

Source: made by the author with the QGIS 3.2.0 'Bonn' program and the OTAB database based on *Zólyomi* 1989 using an SRTM 90 m Digital Elevation Model (*Jarvis et al.* 2008. http://srtm.csi.cgiar.org [Accessed: 20 April 2019.])

[20] *Zólyomi* 1989. 89.

[21] *Járainé* 2006.

The identified species correspond to the potential tree types on the possible vegetation map and the current distribution data of the species.[22] It is a common species in mesophilic and xero-mezophilic oak forests (e.g. hornbeam and sessile oak forests,[23] as well as scrub and low forests[24]).

Taking a look at the surroundings of the site depicted by the First, Second, and Third Military Surveys and topographic maps made before World War II, we find that the vegetation of the area had significantly changed by the eighteenth century. However, there were still accessible forests in riverside areas and on higher terrain, even within distances of 2 to 5 km. Therefore, the obtaining of timber for construction of the well could not have caused any difficulties.

Reviewing the results of the wood analysis, it can be concluded that the examined elements of the well were probably made from the trunks of sessile oak specimens. These trees presumably grew in an area of favourable conditions. What is more, it is also imaginable that they came from the same habitat – based on the growth trends indicated by the widths of annular rings *(Figure 38). Table 16* displays the annual ring widths of the examined specimens in a table format, numbered from core to bark.

The data of the xylotomic analysis are in line with the results of the research carried out by András Grynaeus on the wood remains discovered in the well of Zrínyi-Újvár.[25] Nevertheless, Grynaeus carried out not only a xylotomic but also a dendrochronological analysis.[26] From the results of dating, Grynaeus concluded that the tree the object was made from had most likely been felled after 1658.

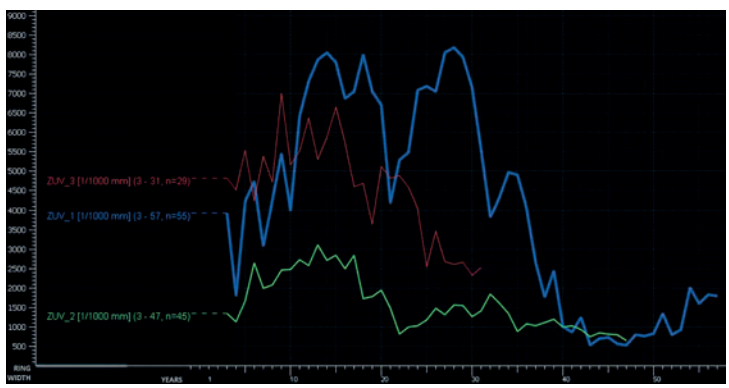

Figure 38.

Annual ring widths of the three samples from the well of the Zrínyi-Újvár archaeological site, and the growth trends calculated from them from core to bark

Source: Saláta 2018.

22 *Bartha et al.* 2015.

23 *Engloner–Penksza–Szerdahelyi* 2001; *Bölöni–Molnár–Kun* 2011.

24 *Simon* 2000.

25 *Grynaeus* 2018.

26 Dendrochronology is a natural scientific auxiliary discipline to archaeology that can identify the age of wood remains with the help of annual rings preserved in trees.

Table 16.

The widths of annual rings numbered from the core to bark [data given in 1/1,000 mm]

Years	Sample 1	Sample 2	Sample 3
3	3,935	1,362	4,826
4	1,806	1,149	4,522
5	4,226	1,681	5,543
6	4,742	2,660	4,239
7	3,097	2,000	5,391
8	4,258	2,085	4,717
9	5,452	2,468	7,000
10	4,000	2,489	5,174
11	6,419	2,745	5,522
12	7,323	2,596	6,370
13	7,871	3,128	5,304
14	8,065	2,723	5,870
15	7,806	2,851	6,652
16	6,871	2,511	5,739
17	7,065	2,851	4,609
18	8,000	1,745	4,696
19	7,065	1,787	3,652
20	6,710	1,957	5,130
21	4,194	1,489	4,826
22	5,290	830	4,891
23	5,484	1,000	4,587
24	7,097	1,043	4,065
25	7,194	1,191	2,565
26	7,065	1,489	3,478
27	8,065	1,319	2,696
28	8,194	1,574	2,630
29	7,935	1,553	2,674
30	7,161	1,277	2,348
31	5,548	1,426	2,543
32	3,839	1,851	
33	4,323	1,617	
34	4,968	1,362	
35	4,903	894	
36	4,065	1,085	
37	2,677	1,043	
38	1,774	1,128	
39	2,452	1,213	
40	1,032	1,000	
41	871	1,043	
42	1,258	936	
43	548	766	
44	710	851	

Years	Sample 1	Sample 2	Sample 3
45	742	830	
46	581	809	
47	548	660	
48	806		
49	774		
50	839		
51	1,355		
52	806		
53	935		
54	2,032		
55	1,613		
56	1,839		
57	1,806		

Source: Saláta 2018.